# Fractal iso-level sets in high-Reynolds-number scalar turbulence

Kartik P. Iyer,[1] Jörg Schumacher,[2,1] Katepalli R. Sreenivasan,[1,3,*] and P. K. Yeung[4]
[1]*Tandon School of Engineering, New York University, New York, New York 11201, USA*
[2]*Institut für Thermo-und Fluiddynamik, Technische Universität Ilmenau, Postfach 100565, D-98684 Ilmenau, Germany*
[3]*Department of Physics and the Courant Institute of Mathematical Sciences, New York University, New York, New York 10012, USA*
[4]*Schools of Aerospace and Mechanical Engineering, Georgia Institute of Technology, Atlanta, Georgia 30332, USA*

(Received 1 October 2019; accepted 14 February 2020; published 27 April 2020)

We study the fractal scaling of iso-level sets of a passive scalar mixed by three-dimensional homogeneous and isotropic turbulence at high Reynolds numbers. The scalar field is maintained by a linear mean scalar gradient, and the Schmidt number is unity. A fractal box-counting dimension $D_F$ can be obtained for iso-levels below about three standard deviations of the scalar fluctuation on either side of its mean value. The dimension varies systematically with the iso-level, with a maximum of about $8/3$ for the iso-level at the mean scalar value; this maximum dimension also follows as an upper bound from the geometric measure theory. We interpret this result to mean that mixing in turbulence is incomplete. A unique box-counting dimension for all iso-levels results when we consider the spatial support of the steep cliffs of the scalar conditioned on local strain rate; that unique dimension, independent of the iso-level set, is about $4/3$.

DOI: 10.1103/PhysRevFluids.5.044501

## I. INTRODUCTION

Consider a homogeneous and isotropic turbulence field in a periodic box at a high Reynolds number, generated by direct numerical simulations (DNS) of the Navier-Stokes (NS) equations. The turbulent field is maintained statistically stationary by supplying energy at a few low-wave-number shells. Into this turbulence field we introduce passive scalar fluctuations statistically homogeneously and allow them to evolve according to the advection diffusion equation along with the NS equations; the scalar field is maintained steady by means of a constant scalar gradient in one direction. For clarity, scalars are quantities that can be specified by their amplitude alone, and passive scalars do not influence the dynamics of turbulence that advects it. The diffusivity of the scalar D is small and equal to the viscosity $\nu$ of the fluid (i.e., the Reynolds number is large and the Schmidt number, $\mathrm{Sc} = \nu/\mathrm{D}$, is unity). Modestly heated air flows form concrete examples close enough to the situation at hand. The properties of passive scalar fields with a variety of Schmidt numbers have been explored in a few classical papers in the late 1940s to mid-1950s [1–3]; summaries of the progress made since then, and references to important papers on the subject, can be found in Refs. [4–8].

Figure 1 shows a typical planar section of the passive scalar field just described. Its first conspicuous property is the presence of large-scale fronts, often called a ramp-cliff structure (see, e.g., Refs. [4,9]) or "cliffs" because of the tendency of the scalar to rise to the high concentration value rather abruptly while decaying to the lower concentration value rather gradually ("ramp");

*krs3@nyu.edu

 

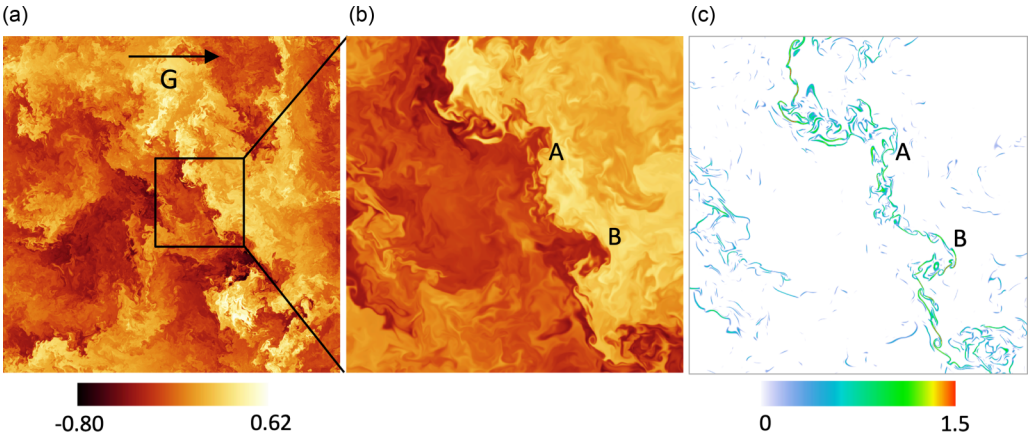


FIG. 1. A two-dimensional slice of the passive scalar fluctuation field $\theta$ in the homogeneous isotropic turbulent flow. In (a) the contours of the cut are shown, as is the direction of the mean scalar gradient $G$; (b) shows the magnification of the contours within the black square in panel (a). Two segments of a scalar front are highlighted by A and B. The color bar below (a) holds for both (a) and (b) in units of $GL_0$, which is the maximum available difference of the mean scalar in the box. (c) The corresponding zoom of the scalar dissipation field, $\epsilon_\theta = D(\nabla\theta)^2$ in units of $u'G^2L_0$, probes the magnitude of the scalar gradient. The contour levels are chosen in units of the logarithm to base 10 of $\epsilon_\theta$ and correspond to the color bar below (c).

across a cliff the nearly abrupt jump of the concentration of the scalar is on the order of magnitude of the entirety of the scalar difference available in the box. This latter is equal to the product of the mean scalar gradient, $G$, and the linear dimension of the box, $L_0$. These fronts occur even when the velocity field is turbulent, and the scalar has the full band of standard spectral shape that we have come to expect [8]. The existence of such sharp and large fronts endows the scalar field with certain types of anomaly studied most recently in Ref. [10] (see also Refs. [11,12] for the two-dimensional case). Briefly, we find that the scaling exponents of the scalar structure functions approach constant values even when the order of the structure function increases without bound. This behavior is unexpected from the classical point of view and is a property shared with model problems such as the Burgers equation for pressureless velocity fields (for a review, see, Ref. [13]) and the Kraichnan model [14] wherein the mixing velocity is a rapidly oscillating Gaussian field.

The second property to which we draw attention is that such fronts consist of convolutions on many scales (see Fig. 1). For example, an enlarged view of Fig. 1(a), shown in Fig. 1(b), has the same qualitative features; see the segment indicated by AB. Indeed, the gradient of the passive scalar shows even more clearly that the front consists of many scales, and an enlargement of its part is similar to the entire scalar gradient field. This feature is displayed in Fig. 1(c). One can visually appreciate that the fronts, more specifically the iso-level sets, contain convolutions over a number of scales. Here iso-level set means the set in three-dimensional space corresponding to fixed levels (or thresholds) of the scalar. For determining an iso-level set for a chosen level, we take a small band of scalar values around that level; in the Appendix we describe how the band thickness was determined. An obvious expectation, then, is that a fractal-like description [15] holds for such iso-level sets. It was first explored much more concretely in Ref. [16–19] and later by others, cited fully in a recent work [20]. A box-counting dimension (which will be defined later) of $D_F = 7/3$ was directly connected in Refs. [17,21,22] to the classical Kolmogorov scaling of velocity increments in turbulence by rate equation models for iso-level segments; it should be pointed out that the models discussed in these references predict the box-counting dimension independent of the iso-level set. Recent DNS [23] for $0.1 \leqslant \mathrm{Sc} \leqslant 7$ and at varying Reynolds numbers have revealed an interesting result that the area of the scalar iso-surface varies as $P_\lambda^{1/2}$ where $P_\lambda \equiv R_\lambda \mathrm{Sc}$ is the microscale Péclet

number and $R_\lambda$ is the microscale Reynolds number. Our study here focuses on a detailed analysis of this property of scalar iso-level sets in relation to the ramp-cliff structure of the fronts. The study will be based on high-resolution DNS data of passive scalar turbulence, described next.

## II. TURBULENCE SIMULATIONS

We use data from pseudospectral DNS of homogeneous isotropic turbulence, computed on $4096^3$ grid points in a periodic cubical box of size $L_0 = 2\pi$ [24]. The passive scalar ($\Theta$) is evolved in the same box using the advection diffusion equation in the presence of a uniform mean gradient $\boldsymbol{G} \equiv (G, 0, 0)$ along the $x$ direction (for specificity), where $G \neq 0$ is a constant, such that $\Theta = \theta + Gx$ and $\theta$ is the scalar fluctuation field. The velocity field $\boldsymbol{u}$ is incompressible and satisfies the NS equations. The equations of motion are

$$\boldsymbol{\nabla} \cdot \boldsymbol{u} = 0, \tag{1}$$

$$\frac{\partial \boldsymbol{u}}{\partial t} + (\boldsymbol{u} \cdot \boldsymbol{\nabla})\boldsymbol{u} = -\boldsymbol{\nabla} p + \nu \boldsymbol{\nabla}^2 \boldsymbol{u} + \boldsymbol{f}, \tag{2}$$

$$\frac{\partial \theta}{\partial t} + (\boldsymbol{u} \cdot \boldsymbol{\nabla})\theta = D\boldsymbol{\nabla}^2 \theta - u_x G, \tag{3}$$

with the large-scale forcing $\boldsymbol{f}$ sustaining a statistically stationary flow; $p$ is the (kinematic) pressure. The microscale Reynolds number $R_\lambda = 650$. In total, we have used more than 30 essentially independent temporal snapshots spanning more than 10 eddy turnover times $T_E \equiv L/u'$, where $u'$ is the root-mean-square velocity fluctuation and $L$ is the integral scale with $L/L_0 \approx 0.2$. The ratio of the root-mean-square scalar fluctuation $\theta'$ to the the maximum available mean scalar difference for this box is $\theta'/GL_0 \approx 0.2$. The spectral resolution is chosen such that $\Delta/\eta = 1.1$, where $\Delta$ is the grid spacing and $\eta$ is the Kolmogorov length $= (\nu^3/\langle\epsilon\rangle)^{1/4}$, and $\langle\epsilon\rangle$ is the mean kinetic energy dissipation rate. An inertial subrange in agreement with Kolmogorov's 4/5-ths law is established for scales approximately between $30\eta$ and $300\eta$. In total, a linear scale range from $\eta$ up to about $2000\eta$ is captured. For further details on the numerical resolution, inertial range properties and statistical convergence, see Refs. [10,25].

## III. BOX-COUNTING ANALYSIS OF DIFFERENT ISO-LEVEL SETS OF THE SCALAR

Fractals are spatial objects that follow a self-similar scaling in the form of power laws [15,18]. An experimental realization of a fractal requires a significant range of scales. In a homogenous turbulent flow, the available scale range varies as $L/\eta \approx \mathrm{Re}^{3/4}$ where the flow Reynolds number is given by $\mathrm{Re} = u'L/\nu$. A fractal scaling with a box-counting dimension $D_F$ exists if the number $N(r)$ of boxes with edge-length $r$ cover an object, in this instance a chosen iso-level set, with the scaling law

$$N(r) = N(L)\left(\frac{r}{L}\right)^{-D_F} \tag{4}$$

for some significant range of scales. The early experiments [16] were for inhomogeneous flows, typically at modest Reynolds numbers, with some attendant uncertainties of scaling. Here we have on hand fully resolved three-dimensional data that span a range of scales that is three orders of magnitude larger. The scale range of the simulation data is also much larger than those of previous simulations such as Refs. [26–28].

Figure 2(a) shows the box-counting result for three iso-levels, corresponding, respectively, to the mean value of the passive scalar, $\theta = 0$, $1.5\theta'$ away from the mean, and, finally, to $3\theta'$ away from the mean. For small $r$, the number of boxes $N(r)$ varies as $r^{-2}$, as should be expected for a spatially smooth field. For $r$ close to $L$, $N(r) \sim r^{-3}$, which shows the space-filling character of the scalar front at the largest scales. In an intermediate range of scales of the order of a decade, $N(r) \sim r^{-D_F}$,

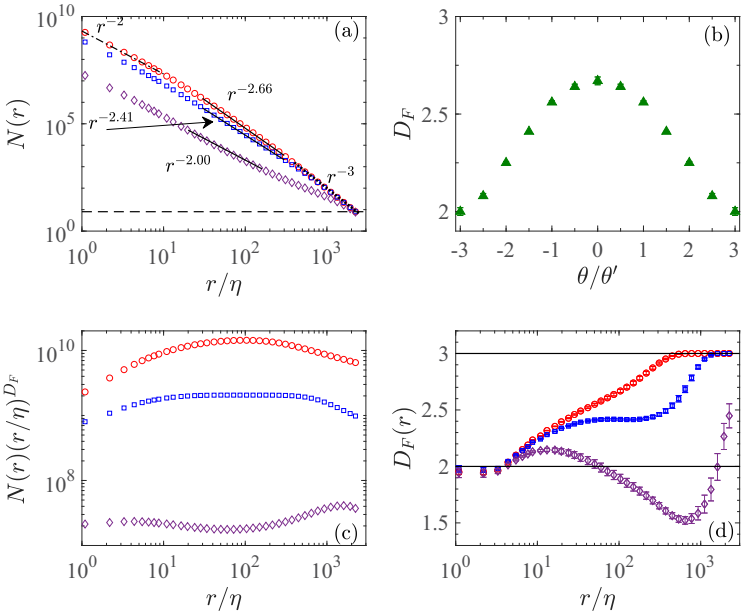


FIG. 2. Box-counting results for scalar iso-levels for $\tilde{\theta} = \theta/\theta'$ of 0 (red circles), 1.5 (blue squares), and 3 (purple diamonds). These symbols have the same meaning in panels (a), (c), and (d). The results are averaged for equal iso-levels of positive and negative $\theta$. (a) The number of boxes $N(r)$ required to cover different iso-levels $\theta/\theta'$ versus box size $r$. The box count is evaluated as $N(r) = \langle N(r)\rangle (L_0/r)^3$, where $\langle N(r)\rangle$ is the average box number from a gliding-box algorithm [29]. The box count obtained by considering nonoverlapping boxes is in good agreement with that from the gliding-box algorithm. Dashed horizontal line at 8 corresponds to $N(r)$ at $r = L_0/2$, which yields the box-counting dimension $D_F = 3$ for $r \sim L_0$, shown by the dotted line. Also shown is the fractal dimension $D_F = 2$ for diffusive scales by the dash-dot line. The power laws in the intermediate scale range are marked by solid lines. (b) The box-counting dimension $D_F$ as a function of the iso-level in the region $|\tilde{\theta}| \leqslant 3$. (c) Double-logarithmic plot of $N(r)$ compensated by $(r/\eta)^{D_F}$ versus $r/\eta$, where $D_F$ is obtained from (a) using the method of least-squares. (d) Logarithmic local slope $D_F(r) = -d[\log N(r)]/d[\log r]$ of three different iso-levels $\tilde{\theta}$. Solid horizontal lines drawn for ordinate values 2 and 3 denote the small- and large-scale dimension limits, respectively.

where $2 \leqslant D_F \leqslant 3$. Only three iso-level sets are shown in Fig 2(a) for reasons of clarity. We will examine the quality of these fits in the next paragraph, but if we plot the dimension $D_F$ obtained from linear fits in the double-logarithmic plots, against the iso-level values $\tilde{\theta} \equiv \theta/\theta'$, we find a continuous variation from 2 for iso-levels that are far away from the mean to about 2.67 for the iso-level corresponding to the mean of $\theta$ [see Fig. 2(b)]. That the dimension is $D_F \approx 2$ for iso-level sets with large thresholds is obvious because essentially no mixing has taken place that far away from the mean, and hardly any mixing front is available for larger thresholds than about $3\theta'$. We will comment separately on the peak value of the dimension.

The quality of the power laws has been a matter of contention (see, e.g., discussions in Refs. [6,18]), so we explore this issue further, first by showing, in Fig. 2(c), the compensated plots using the $D_F$ values obtained in Fig. 2(a). There is a very clear plateau for $\tilde{\theta} = 1.5$, for $D_F = 2.35$, as was also found in the past analyses of experimental [16] and DNS [27] data; this is also reasonably true for $\tilde{\theta} = 3$ for which $D_F = 2$ because the scalar with such large deviations from the mean has essentially not mixed, with no chance of developing a contorted front. For $\theta = 0$, however, there is at best a hint of a plateau—a point to which we shall return later. In addition, we show in Fig. 2(d) the corresponding local slopes. Again, it is clear that local slopes have a region of satisfactory constancy for $\tilde{\theta} = 1.5$, perhaps roughly so (on the average) also for $\tilde{\theta} = 3$, but possess just a hint of

inflection for the iso-level of 0. Incidentally, most past skeptics of power laws have focused on the case $\theta = 0$. The rest of the paper is mostly an effort to understand the results of Fig. 2, and connect them, qualitatively, with the ramp-cliff structure.

## IV. UPPER LIMIT TO SCALING DIMENSION BY GEOMETRIC MEASURE THEORY

We now consider the case of zero iso-level for which, as discussed already, there is only a hint of an inflection in local slope. In Ref. [30] it was shown by geometric measure theory—which is the generalization to rough surfaces of the method for calculating the area content of a curved surface—and the standard hypothesis that velocity increments in classical turbulence are Hölder continuous with an exponent of 1/3, that a scalar interface is indeed a fractal with the dimension $D_F$ of 8/3. By drawing lines in log-log plots as in Fig. 2, Constantin *et al.* [30] deemed that the dimension was supported experimentally [18] to be 8/3. A dimension of 8/3 also follows if the procedure used in [18,20], based on flux estimates, is extended by stipulating that scalar increments $\delta_r\theta$ in the inertial convective range follow the standard scaling of $r^{1/3}$. Since, as we have seen, the evidence for it is not as clean as for other iso-levels, we now examine this issue in greater detail.

We first describe the geometric measure theory [31] result briefly. The central object of interest is the scaling behavior of the Hausdorff volume $H$ of a passive scalar graph over a three-dimensional ball $B_r$ with radius $r$v and volume $V = 4\pi r^3/3$; it is given [30,32] by

$$H(g(B_r)) \sim r^{D_g}, \tag{5}$$

with the graph $g$ over the sphere, defined at a particular time instant as $g(B_r) = \{(\boldsymbol{x}, \theta)|\boldsymbol{x} \in B_r \text{ and } \theta = \theta(\boldsymbol{x})\}$. Here $D_g$ is the scaling dimension of the graph, which is by definition connected to the fractal dimension $D_F$ by

$$D_F = D_g - 1. \tag{6}$$

For the derivation of $D_g$ we follow Ref. [32] (see also Ref. [33] for a two-dimensional case). According to the theory, the relative Hausdorff volume is given by

$$\frac{H(g(B_r))}{V} = \frac{1}{V}\int_{B_r}\sqrt{1 + r^2|\nabla\tilde{\theta}|^2}\,dV \leqslant \sqrt{1 + \frac{3}{4\pi r}\int_{B_r}|\nabla\tilde{\theta}|^2\,dV}. \tag{7}$$

The expression in the middle of (7) is the generalization of the formula for calculating the length of a curve. As before, $\tilde{\theta} = \theta/\theta'$. The second step follows from the Cauchy-Schwarz inequality. As discussed in Ref. [30], further progress can be made by substituting for the square of the scalar gradient by the appropriate terms of the underlying advection-diffusion equation (3) of the passive scalar $\theta$. In the statistically stationary regime, one obtains, by the multiplication of this equation with $\theta$ and a subsequent integration by parts, the following expression:

$$|\nabla\tilde{\theta}|^2 = -\frac{1}{2D}(\boldsymbol{u}\cdot\nabla)\tilde{\theta}^2 + \frac{1}{2}\nabla^2\tilde{\theta}^2 - \frac{u_x G\tilde{\theta}}{D\theta'}. \tag{8}$$

In Ref. [32] it was shown that the second and third terms on the right-hand side of (8) are bounded by the first term. The first term itself can be rewritten as an expression that contains the second-order structure function of longitudinal velocity increment $S_\parallel(r)$. In deriving the final result given by

$$\frac{H(g(B_r))}{V} \leqslant \sqrt{1 + \frac{3\sqrt{3}}{2}\tilde{r}\sqrt{\tilde{S}_\parallel(\tilde{r})}}, \tag{9}$$

one uses the homogeneity of the scalar turbulence and the Cauchy-Schwarz inequality once more. In addition, it uses the result that the scalar flatness takes the value $F_{\tilde{\theta}} = \langle\tilde{\theta}^4\rangle \approx 3$, which has been shown, for example, in Refs. [28,34]. Here, $\tilde{r} \equiv r/\eta$ and $\tilde{S}_\parallel \equiv S_\parallel/v_\eta^2$, where $v_\eta = (\nu\langle\epsilon\rangle)^{1/4}$ is the Kolmogorov velocity. Further details on the derivation of the formula can be found in Refs. [32,33].

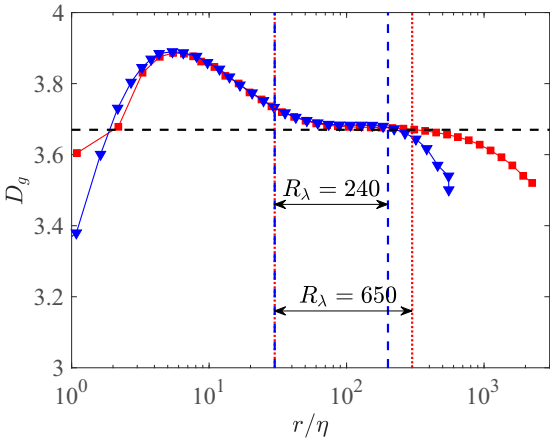


FIG. 3. Local scaling dimension of the Hausdorff volume $D_g(\tilde{r})$ versus $r/\eta$. The quantity is obtained for a passive scalar graph over a three-dimensional ball $B_r$ of varying radius $r$ for $R_\lambda = 650$ (squares) and for an additional DNS run at $R_\lambda = 240$ (inverted triangles). In the inertial range (demarcated by the vertical lines), $D_g = 11/3$, indicated by the horizontal dashed line, and is consistent with the fractal dimension of 2.67 for the zero iso-level shown in Fig. 2.

From Eq. (9) follows the local slope

$$D_g(\tilde{r}) = 3 + \frac{d}{d\log\tilde{r}} \log\sqrt{1 + \frac{3\sqrt{3}}{2}\tilde{r}\sqrt{\tilde{S}_\parallel(\tilde{r})}}, \tag{10}$$

where we assume that the inequality can be replaced by an equality. If we assume that the inertial range scaling exponent of the longitudinal structure function to be 2/3 (as is thought to hold for Kolmogorov turbulence—with slight intermittency correction if needed [35]), we find from (10) that $D_g = 11/3$. We plot in Fig. 3 the results that follow when the structure function from the DNS is inserted. For comparison, we add another data record at $R_\lambda = 240$. The power-law scaling is not very extended, but a range of scales certainly exists for which $D_F$ is close to 8/3 (indicated by the dashed line at $D_g = 11/3$). Our whole analysis in this section did not make any assumption on the particular level set. We can thus interpret the resulting box-counting dimension given by (6) as an upper bound $\overline{D}_F$. In other words, a passive scalar in a three-dimensional flow can be stirred and advected in the inertial subrange only to level set with $D_F \leqslant \overline{D}_F$. Our analysis in Fig. 2(b) clearly supports this bound.

## V. UNIQUE MONOFRACTAL SCALING IN STRAIN-DOMINATED CLIFF REGIONS

Our box-counting analysis in Sec. III revealed that different scalar iso-level sets show different scaling dimensions. We might therefore ask if a unique monofractal can be observed under any circumstances at all. The cliff regions, i.e., the regions in which the magnitude of $\partial\theta/\partial x$ is large, already satisfy this expectation roughly. In Ref. [10] we have identified a box-counting dimension of $D_F = 1.8$ for the spatial support for this particular subset of the whole volume. Figure 4 highlights these regions as red points in a total scalar fluctuation profile $\theta + Gx$ (blue line) taken across the diagonal of Fig. 1(a). The bottom panel of this figure illustrates the selection criterion by which we identify the scalar derivative with the strongest spatial variations. We found in Ref. [10] that the scalar iso-levels corresponding to these spatial regions have a box-counting dimension of $D_F \leqslant 1.8$, which suggests that the cliffs are loosely in the form of a surface with holes.

But one can do better in terms of the quality of scaling by restricting attention on cliff regions connected to a persistent local straining motion, a known process studied in the chaotic mixing

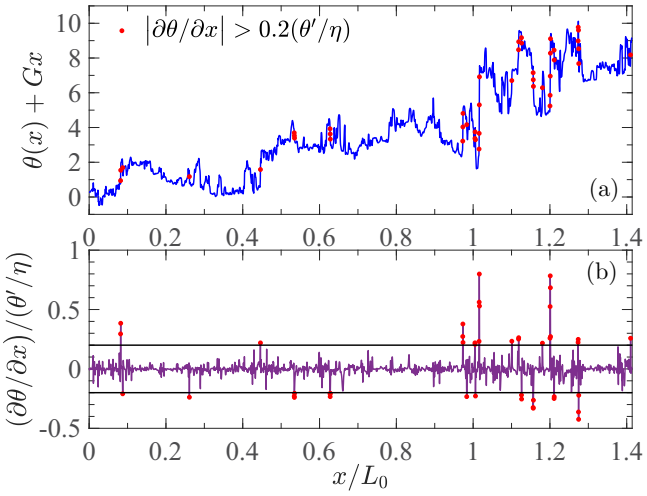


FIG. 4. Scalar cliff region identification. (a) The line trace taken diagonally across the data shown in Fig. 1 (a) from the lower left to the upper right corner. Red points indicate the positions at which the derivative magnitude $|\partial\theta/\partial x|$ exceeds the threshold given in the legend. The criterion is taken from Ref. [10]. The mean scalar gradient is added to show the ramp-cliff structure more clearly. (b) The corresponding derivative trace $\partial\theta/\partial x$ in units of $\theta'/\eta$ along the same diagonal as (a), indicating that the highest amplitudes are captured by this criterion.

regime of high-Schmidt-number turbulence [36–38]. For this purpose, we refine the analysis and examine strain-dominated subsets in the cliff regions. They are extracted from a local eigenvalue analysis of the velocity gradient tensor $\boldsymbol{\nabla u}$ (at every grid point); see Refs. [39,40]. The dominance

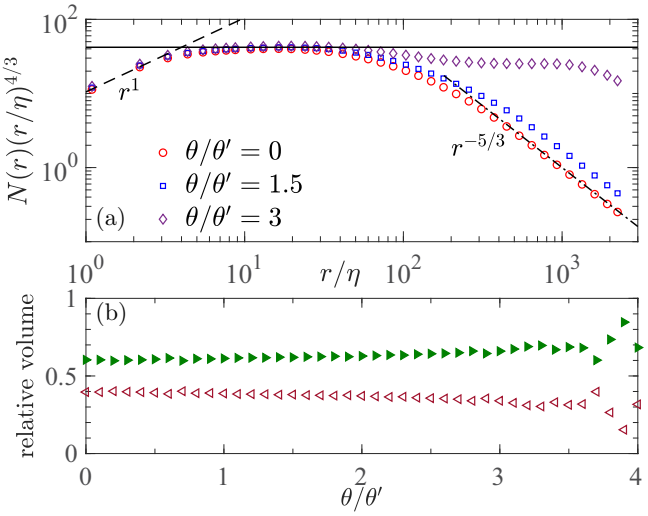


FIG. 5. Scaling of scalar iso-level conditioned on the high strain rate of the cliffs. (a) The compensated log-log plot of $N(r)$ versus size $r$, for the strain-dominated regions of the flow. The plateau region marked by the solid line corresponds to the $4/3$ scaling and is exhibited by all iso-levels sets shown. The small- and large-scale regimes exhibit a $-1/3$ (dashed line) and $-3$ (dash-dot line) scaling dependency, respectively. (b) Relative volume fraction of strain-dominated (filled triangles) and rotation-dominated regions (open triangles) for the chosen scalar iso-level set $\theta/\theta'$. This analysis relates to the strain-dominated cliff regions only with ($|\partial\theta/\partial x| > 0.2\theta'/\eta$).

of local pure strain (as opposed to local rotation) implies that the velocity gradient tensor is locally symmetric and possesses three real eigenvalues that sum up to zero due to incompressibility. Box-counting results for these regions are shown in Fig. 5. We find in Fig. 5(a) that for all iso-levels the scaling is uniformly the same and approximately $4/3$, suggesting that the strain dominated regions of the cliff are better regarded as highly convoluted line-like objects rather than surfaces full of holes. Figure 5(b) shows the relative volumes of the strain- and rotation-dominated regions in the spatial support of the cliffs, which have to sum up to unity; these results are the outcome of the eigenvalue analysis of the velocity gradient tensor. It is seen that the volume fractions do not change much with the value of the iso-level. The conclusion is that in strain-dominated regions of the spatial support of the cliffs, there is a unique fractal scaling dimension for all iso-level sets, and its value is approximately $4/3$. Such a box-counting dimension could correspond to material lines that are most probably stirred by velocity increments in the inertial range, characterized by the spatial scaling of $r^{1/3}$.

Finally, we may now turn to the physical meaning of the upper bound of about 2.67 for the fractal dimension of the iso-scalar surfaces, which corresponds to $\theta = 0$. This shows that such levels sets are not space filling in the inertial range. If perfect mixing occurs in the inertial range, such a surface would have a space-filling dimension of 3. Given that the regions where mixing has been accomplished on inertial-range scales are only $8/3$, we conclude that there is an upper bound to the mixing in turbulent flows [8]. It would be rewarding to prove this result analytically. The presence of strong ramp-cliff structures at even the highest Reynolds numbers considered here is completely consistent with this view of incomplete mixing with a finite bound.

## VI. CONCLUSIONS

We have conducted a geometric analysis of passive scalar iso-level sets in three-dimensional turbulence at high Reynolds numbers and a Schmidt number $\mathrm{Sc} = 1$. The homogeneous and isotropic box turbulence advecting the flow is characterized by an inertial range over an order of magnitude in which the Kolmogorov $4/5$-ths law holds, as shown in Ref. [10]. Furthermore, the Kolmogorov scale $\eta$ is resolved with one grid spacing, which provides a high-quality DNS data set as the basis of analysis.

We have shown that a box-counting scaling dimension $D_F$ can be obtained for all iso-levels, excepting those for high amplitudes, say, $|\tilde{\theta}| > 3$, because there is essentially no mixing at such high iso-levels and the front, such as may exist, has very little likelihood of developing any contortions that lead to fractal scaling. Below that threshold level, the box-counting dimension $D_F$ varies with the iso-level magnitude.

By means of geometric measure theory, we derived an upper bound $D_F \leqslant 8/3$ which is the maximum possible dimension of the iso-level sets; this corresponds to the iso-level set of zero, towards which all mixing processes are driven. If the mixing were complete, the zero iso-level sets would be space-filling, and we would obtain a dimension of 3. The fact that we do not achieve this condition suggests that the mixing is not complete in a turbulent flow. This is because there is a finite probability of encountering cliffs across which the scalar jumps by almost the amount allowed in the flow. Expressed differently, there are always positions in the flow where the lowest concentrations of the scalar are separated by the highest concentration levels only by the smallest scale available to the flow. That this happens for the case of homogeneous and isotropic turbulence suggests that it must be a general feature of turbulence, which leads us to conclude that there is an upper bound to turbulent mixing in practice.

We already noted that the box-counting dimension $D_F$ varies with the iso-level magnitude and that a unique monofractal behavior with a scaling dimension independent of the iso-level is not obtainable. However, such a unique monofractal scaling of scalar iso-levels can be obtained when two additional conditions are imposed: (1) select those points of space that spatially support the steep scalar cliffs, and (2) condition the box-counting analysis of iso-levels on this support to high-strain events. In some sense, this is the backbone of structures that prevent complete scalar mixing.

An extension of this analysis for high-Schmidt-number passive scalar turbulence can be considered as the natural next step. A first step of the Schmidt-number dependence within the framework of geometric measure theory was already presented in Ref. [41]. A more extensive study is currently under way and will be reported elsewhere.

## ACKNOWLEDGMENTS

The computations and data analyses reported in this paper were performed using advanced computational facilities provided by the Texas Advanced Computation Center (TACC) under the XSEDE program supported by the US National Science Foundation under Grant No. ACI-1036170. The data sets used were originally generated using supercomputing resources at the Oak Ridge Leadership Computing Facility at the US Department of Energy Office of Science user facility supported under Contract No. DE-AC05-00OR22725 Oak Ridge National Laboratory. We thank Dr. Inigo San Gil for his involvement 20 years ago in this project using low-resolution data, Prof. Diego Donzis for his initiative on the high-resolution passive scalar simulations reported here, and Prof. Charles Meneveau for useful comments. J.S. wishes to thank the Tandon School of Engineering at New York University for financial support.

## APPENDIX: THE DEFINITION OF THE SCALAR ISO-LEVEL THICKNESS

Consider passive scalar fluctuation $\theta$ with diffusivity $D_\phi$, mean scalar dissipation $\epsilon_\theta$, and Schmidt number $\mathrm{Sc} = \nu/D_\phi$ where $\nu$ is the kinematic viscosity of the advecting fluid. The typical scalar variation across grid cell $\delta = L_0/N$ in a cube with edge length $L_0$ with $N$ points to a side can be written as

$$\delta\theta = \left(\frac{\epsilon_\theta}{D_\phi}\right)^{1/2}\delta. \tag{A1}$$

Denoting the small-scale resolution parameter $k_{\max}\eta_B$ by $C$, where $k_{\max}$ is the highest resolvable wave number in a $N^3$ simulation with smallest nonzero wave-number magnitude $k_0 = 2\pi/L_0$ and $\eta_B$ is the Batchelor scale $\eta_B = \eta/\mathrm{Sc}^{1/2}$, we can write

$$C = \frac{\sqrt{2}}{3}Nk_0\eta_B = \frac{\sqrt{2}}{3}\left(\frac{L_0}{\delta}\right)\left(\frac{2\pi}{L_0}\right)\eta_B. \tag{A2}$$

Solving for $\delta$ in the above equation, substituting into Eq. (A1) and dividing both sides by the root-mean-square scalar fluctuation $\theta'$ we get

$$\frac{\delta\theta}{\theta'} = \left(\frac{\epsilon_\theta}{D_\phi}\right)^{1/2}\frac{1}{\theta'}\frac{2\sqrt{2}\pi}{3C}\eta_B\,. \tag{A3}$$

Assuming dissipative anomaly for the scalar field in isotropic turbulence [42] we can write

$$\epsilon_\theta = A[1+\sqrt{1+(B/R_\lambda)^2}]\frac{\theta'^2 u'}{L}, \tag{A4}$$

where $u'$ is the root-mean-square velocity fluctuation, $L$ is the flow integral scale, and $A$ and $B$ are constants that depend on the Schmidt number [42]. Substituting Eq. (A4) into Eq. (A3) and rearranging we get

$$\frac{\delta\theta}{\theta'} = \frac{2\sqrt{2}\pi}{3C}\{A[1+\sqrt{1+(B/R_\lambda)^2}]\}^{1/2}(\mathrm{Re}\,\mathrm{Sc})^{1/2}\left(\frac{\eta_B}{L}\right), \tag{A5}$$

where Re and $R_\lambda$ denote the Reynolds numbers based on the integral scale and the Taylor microscale, respectively, and are related to each other in isotropic turbulence as $R_\lambda = (\frac{20}{3}\mathrm{Re})^{1/2}$. For $\mathrm{Sc} = 1$,

$\eta_B = \eta$ and thus we can finally write

$$\frac{\delta\theta}{\theta'} = \frac{2\sqrt{2}\pi}{3C}\{A[1+\sqrt{1+(B/R_\lambda)^2}]\}^{1/2}\left(\frac{20}{3}\right)^{1/4} R_\lambda^{-1/2}. \tag{A6}$$

For a resolution of $N^3 = 4096^3$ in our DNS with $R_\lambda = 650$ and $C = 2.72$, substituting $A \approx 0.4$ and $B \approx 31$, it follows that the iso-level thickness is effectively

$$\pm\delta\theta/\theta' \approx \pm 0.03, \tag{A7}$$

for the present data. In the final analysis, this is a rough estimate only.


[1] A. M. Obukhov, Structure of the temperature field in a turbulent flow, Izv. Akad. Nauk SSSR, Ser. Geogr. Geofiz. **13**, 58 (1949).

[2] S. Corrsin, On the spectrum of isotropic temperature fluctuations in an isotropic turbulence, J. Appl. Phys. **22**, 469 (1951).

[3] G. K. Batchelor, Small-scale variation of convected quantities like temperature in turbulent fluid Part 1. General discussion and the case of small conductivity, J. Fluid Mech. **5**, 113 (1959).

[4] K. R. Sreenivasan, On local isotropy of passive scalars in shear flows, Proc. R. Soc. London A **434**, 165 (1991).

[5] Z. Warhaft, Turbulence in nature and in the laboratory, Proc. Natl. Acad. Sci. USA **99**, 2481 (2002).

[6] P. E. Dimotakis, Turbulent mixing, Annu. Rev. Fluid Mech. **37**, 329 (2005).

[7] T. Gotoh and P. K. Yeung, Passive scalar transport in turbulence: A computational perspective, in *Ten Chapters in Turbulence*, edited by P. A. Davidson, Y. Kaneda, and K. R. Sreenivasan (Cambridge University Press, Cambridge, 2013), p. 87.

[8] K. R. Sreenivasan, Turbulent mixing: A perspective, Proc. Natl. Acad. Sci. USA **116**, 18175 (2019).

[9] F. Holzer and E. D. Siggia, Turbulent mixing of a passive scalar, Phys. Fluids **6**, 1820 (1994).

[10] K. P. Iyer, J. Schumacher, K. R. Sreenivasan, and P. K. Yeung, Steep Cliffs and Saturated Exponents in Three-Dimensional Scalar Turbulence, Phys. Rev. Lett. **121**, 264501 (2018).

[11] A. Celani, A. Lanotte, A. Mazzino, and M. Vergassola, Universality and Saturation of Intermittency in Passive Scalar Turbulence, Phys. Rev. Lett. **84**, 2385 (2000).

[12] A. Celani, A. Lanotte, A. Mazzino, and M. Vergassola, Fronts in passive scalar turbulence, Phys. Fluids **13**, 1768 (2001).

[13] G. Falkovich, K. Gawędzki, and M. Vergassola, Particles and fields in fluid turbulence, Rev. Mod. Phys. **73**, 913 (2001).

[14] R. H. Kraichnan, Small-scale structure of a scalar field convected by turbulence, Phys. Fluids **11**, 945 (1968).

[15] B. B. Mandelbrot, *Fractals: Form, Chance and Dimension* (W. H. Freeman & Co., New York, 1977).

[16] K. R. Sreenivasan and C. Meneveau, The fractal facets of turbulence, J. Fluid Mech. **173**, 357 (1986).

[17] K. R. Sreenivasan, R. Ramshankar, and C. Meneveau, Mixing, entrainment and fractal dimension of surfaces in turbulent flows, Proc. Roy. Soc. London A **421**, 79 (1989).

[18] K. R. Sreenivasan, Fractals and multifractals in turbulence, Annu. Rev. Fluid Mech. **23**, 539 (1991).

[19] C. Meneveau and K. R. Sreenivasan, Interface dimension in intermittent turbulence, Phys. Rev. A. **41**, 2246(R) (1990).

[20] L. P. Dasi, F. Schuerg, and D. R. Webster, The geometric properties of high-Schmidt-number passive scalar iso-surfaces in turbulent boundary layers, J. Fluid Mech. **588**, 253 (2007).

[21] E. Villermaux and C. Innocenti, On the geometry of turbulent mixing, J. Fluid Mech. **393**, 123 (1999).

[22] E. Villermaux, On shapes and forms: Population balance dynamics of corrugated stirred fronts, C. R. Phys. **19**, 306 (2018).

[23] K. P. Shete and S. M. de Bruyn Kops, Area of scalar isosurfaces in homogeneous isotropic turbulence as a function of Reynolds and Schmidt numbers, J. Fluid Mech. **883**, A38 (2020).

[24] D. A. Donzis, K. R. Sreenivasan, and P. K. Yeung, The Batchelor spectrum for the mixing of passive scalars in isotropic turbulence, Flow, Turb. Combust. **85**, 549 (2010).
[25] P. K. Yeung, D. A. Donzis, and K. R. Sreenivasan, Dissipation, enstrophy and pressure statistics in turbulence simulations at high Reynolds numbers, J. Fluid Mech. **700**, 5 (2012).
[26] A. Brandenburg, I. Procaccia, D. Segel and A. Vincent, Fractal level sets and multifractal fields in direct simulations of turbulence, Phys. Rev. A **46**, 4819 (1992).
[27] I. San Gil, Fractal character of iso-scalar surfaces in shear free turbulence and some effects of shear on the turbulence structure, Ph.D. thesis, Yale University, 2001.
[28] J. Schumacher and K. R. Sreenivasan, Statistics and geometry of passive scalars in turbulence, Phys. Fluids **17**, 125107 (2005).
[29] C. Allain and M. Cloitre, Characterizing the lacunarity of random and deterministic fractal sets, Phys. Rev. A **44**, 3552 (1991).
[30] P. Constantin, I. Procaccia, and K. R. Sreenivasan, Fractal Geometry of Isosurfaces in Turbulence: Theory and Experiment, Phys. Rev. Lett. **67**, 1739 (1991).
[31] F. Morgan, *Geometric Measure Theory: A Beginner's Guide* (Academic Press, San Diego, 2000).
[32] S. Grossmann and D. Lohse, Fractal-dimension crossovers in turbulent passive scalar signals, Europhys. Lett. **27**, 347 (1994).
[33] B. Eckhardt and J. Schumacher, Structure function of passive scalars in two-dimensional turbulence, Phys. Rev. E **60**, 4185 (1999).
[34] M. R. Overholt and S. B. Pope, Direct numerical simulation of a passive scalar with imposed mean gradient in isotropic turbulence, Phys. Fluids **8**, 3128 (1996).
[35] U. Frisch, *Turbulence—The Legacy of A. N. Kolmogorov* (Cambridge University Press, Cambridge, 1995).
[36] D. Kushnir, J. Schumacher, and A. Brandt, Geometry of Intensive Scalar Dissipation Events in Turbulence, Phys. Rev. Lett. **97**, 124502 (2006).
[37] E. Villermaux, Mixing versus stirring, Annu. Rev. Fluid Mech. **51**, 245 (2019).
[38] P. Götzfried, M. S. Emran, E. Villermaux, and J. Schumacher, Comparison of Lagrangian and Eulerian frames of passive scalar turbulent mixing, Phys. Rev. Fluids **4**, 044607 (2019).
[39] W. T. Ashurst, A. R. Kerstein, R. M. Kerr, and C. H. Gibson, Alignment of vorticity and scalar gradient with strain rate in simulated Navier-Stokes turbulence, Phys. Fluids **30**, 2343 (1987).
[40] J. Schumacher, K. R. Sreenivasan, and P. K. Yeung, Very fine structures in scalar mixing, J. Fluid Mech. **531**, 113 (2005).
[41] J. Schumacher, Scalar gradient fields by geometric measure theory, Phys. Rev. E **69**, 047301 (2004).
[42] D. A. Donzis, P. K. Yeung and K. R. Sreenivasan, Scalar dissipation rate and dissipative anomaly in isotropic turbulence, J. Fluid Mech. **532**, 199 (2005).